Muon spin relaxation and susceptibility measurements of an itinerant-electron system $Sr_{1-x}Ca_xRuO_3$: Quantum evolution from ferromagnet to paramagnet

I. M. Gat-Malureanu,[1,2,*] J. P. Carlo,[2,†] T. Goko,[2,3] A. Fukaya,[2] T. Ito,[2,‡] P. P. Kyriakou,[4] M. I. Larkin,[2] G. M. Luke,[4] P. L. Russo,[2] A. T. Savici,[2,§] C. R. Wiebe,[2,4,‖] K. Yoshimura,[5] and Y. J. Uemura[2,*]

[1]*Science Department, SUNY Maritime College, 6 Pennyfield Avenue, Throggs Neck, New York, 10465, USA*

[2]*Department of Physics, Columbia University, 538W 120th St., New York, New York, 10027, USA*

[3]*TRIUMF, 4004 Wesbrook Mall, Vancouver, B.C., V6T 2A3, Canada*

[4]*Department of Physics and Astronomy, McMaster University, 1280 Main St. West, Hamilton, Ontario, Canada L8S 4M1*

[5]*Department of Chemistry, Kyoto University, Kyoto 606-8502, Japan*

(Received 4 February 2011; revised manuscript received 21 November 2011; published 19 December 2011)

Muon spin relaxation (μSR) and magnetic susceptibility measurements have been performed in the itinerant-electron magnet $Sr_{1-x}Ca_xRuO_3$, with $x = 0.0$, 0.3, 0.5, 0.65, 0.7, 0.75, 0.8, 0.9, and 1.0. $SrRuO_3$ is a ferromagnet with the critical temperature $T_c \sim 160$ K. Upon (Sr, Ca) substitution, T_c decreases monotonically with increasing Ca concentration x and the ferromagnetic order disappears around $x = 0.7$. Very weak static magnetism is observed in the $x = 0.75$ and 0.8 systems, while the $x = 0.9$ and 1.0 systems remain paramagnetic in their full volume. Phase separation between volumes with and without static magnetism was observed in the $x = 0.65$, 0.7, 0.75, and 0.8 systems, near the magnetic crossover around $x = 0.7$. In this concentration region, μSR measurements revealed discontinuous evolution of magnetic properties in contrast to magnetization measurements, which exhibit seemingly continuous evolution. Unlike the volume-integrated magnetization measurements, μSR can separate the effects of the ordered moment size and the volume fraction of magnetically ordered regions. The muon spin relaxation rate $1/T_1$ exhibits critical slowing down of spin fluctuations near T_c in the ferromagnetic systems with $x = 0.0$–0.65, consistent with the behavior expected in the self-consistent renormalization theory of itinerant electron ferromagnets. The lack of maximum of $1/T_1$ in the $x = 0.7$ system indicates the disappearance of critical slowing down. These results demonstrate a first-order quantum evolution in the ferromagnet to paramagnet crossover near $x = 0.7$.

DOI: 10.1103/PhysRevB.84.224415 PACS number(s): 75.30.Kz, 73.43.Nq, 76.75.+i

I. INTRODUCTION

Itinerant electron systems $Sr_{1-x}Ca_xRuO_3$ have attracted significant interest of researchers with respect to evolution from ferromagnetic to paramagnetic ground states, which occurs as a function of (Sr, Ca) substitution x. Strontium-calcium perovskite ruthenate systems appear as the Ruddlesden-Popper series $A_{1+n}Ru_nO_{1+3n}$, where A is a divalent cation such as Sr or Ca.[1,2] The $n = 1$ "214" systems, including a prototypical unconventional superconductor Sr_2RuO_4,[3,4] have a single-layered two-dimensional RuO planes. The three-dimensional $n = \infty$ "113" ruthenate systems $Sr_{1-x}Ca_xRuO_3$ stabilize in a nearly cubic but orthorhombic structure of the $GdFeO_3$ type.[5–7] The distortion from the idealized cubic perovskite structure is generated by a tilting of the RuO_6 octahedra due to the smaller size of Ca^{2+} ions relative to Sr^{2+} ions, resulting in greater distortion for larger Ca concentrations. In the two-dimensional 214 ruthenate systems $(Sr_{1-x}Ca_x)_2RuO_4$, this tilting makes the band width narrower, and drives metallic Sr_2RuO_4 into an insulating Ca_2RuO_4.[8,9] Unlike the 214 system, however, the 113 systems remain metallic in the entire composition range of $x = 0.0$ to 1.0.[10,11]

Evolution from localized-moment magnetism to correlated paramagnetism in metallic systems has attracted significant interest since the 1970's. Such an evolution can be found, for example, in a variety of systems including Heusler alloys, Fe, Ni, MnSi, and Pd. The ferromagnetic systems all exhibit Curie-Weiss law in the magnetic susceptibility χ, with substantial "paramagnetic moment" values p_c derived from the Curie constant of χ at high temperatures. The ordered ferromagnetic moment p_s at $T = 0$, however, is significantly reduced from p_c. The Rhodes-Wohlfarth ratio p_c/p_s increases from $\sim$1 in the localized-moment limit to a very large value ($\sim$5.5) in "weak" ferro-/helimagnet MnSi and, finally, diverges in Pd, which loses ferromagnetic order.[12] This evolution also shows up in the ratio of the energy scales of spin fluctuations or spin waves at the zone boundary (which is a measure of an effective exchange interaction J) and of the transition temperature energy scale k_BT_c. Moriya, Kawabata, Doniach, Lonzarich, and others[13–18] have contributed to develop a comprehensive understanding of this evolution. In particular, the self-consistent renormalization (SCR) theory of Moriya and Kawabata has been very successful in describing it and accounting for experimental results in weak ferro- or helical magnets, such as MnSi and $ZrZn_2$. In MnSi, application of hydrostatic pressure has been found[19] to drive the system into a paramagnet. Extensive experimental studies[20–22] have been performed to characterize the quantum crossover from helical to paramagnetic ground states of MnSi as a function of pressure.

$SrRuO_3$ is an itinerant ferromagnet[23] in which long-range magnetic order stabilizes below $T_c \sim 160$ K. The (Sr, Ca) substitution monotonically decreases the critical temperature with increasing x, and the zero-temperature spontaneous moment p_s vanishes at a calcium concentration x close to 0.7, as reported by magnetization measurements.[24,25] Kiyama *et al.*[24] also found that $Sr_{1-x}Ca_xRuO_3$ exhibits Curie-Weiss-like magnetic susceptibility in the whole composition range, with the

Weiss temperature θ changing sign from positive to negative at approximately $x = 0.7$. The paramagnetic moment p_c remains nearly constant, while the ordered moment $p_s(T = 0)$ decreases with increasing x. Based on these observations, Kiyama *et al.*[24] proposed to map the evolution due to (Ca, Sr) substitutions to the above-mentioned general behavior expected by the SCR theory in itinerant-electron systems.

In this view, with increasing Ca concentration, the system evolves from an intermediate itinerant ferromagnet $SrRuO_3$, through weak itinerant ferromagnet, to the nearly ferromagnetic metal $CaRuO_3$, which remains paramagnetic down to $T = 0$ K.[24,26,27] We note that both Sr substitution with Ca as well as application of hydrostatic pressure to $SrRuO_3$[28–30] reduces the unit-cell volume, and results in the reduction of T_c. On the other hand, the Sommerfeld constant γ, derived from the T-linear term of the specific heat,[27] does not show monotonic behavior with (Ca, Sr) substitutions. This observation rules out a simplistic picture that the ferro-para evolution is caused by a band narrowing due to increasing crystal tilting with increasing x, nor by a band widening that can be expected in general when metallic systems are squeezed by hydrostatic pressure. The specific heat study[27] suggested that the increase in γ is not due to an increase in the density of states at the Fermi level, but due to spin fluctuations that enhance specific heat through exchange interactions in the low-temperature region.

We started to perform muon spin relaxation (μSR) measurements of $Sr_{1-x}Ca_xRuO_3$ using polycrystal specimens in 2000. During the course of our study, we also performed measurements of dc and ac magnetization to characterize the specimens used in the μSR studies. Recently, we compared a part of zero-field (ZF) μSR and dc magnetization results on (Sr,Ca)RuO_3 with μSR measurements of MnSi under applied pressure,[22] and reported that quantum evolutions of both MnSi and (Sr,Ca)RuO_3 into paramagnets are associated with phase separations between volumes with and without static magnetism near the boundary existing at the critical pressure of 14.7 kbar in MnSi and at $x \sim 0.7$ in $Sr_{1-x}Ca_xRuO_3$. In MnSi, we also reported disappearance of dynamic critical behavior observed in the muon spin relaxation rate $1/T_1$ near this phase boundary.[22] These are the characteristic behaviors expected for the first-order phase transition between the magnetically ordered and paramagnetic phases.

In this paper, we provide a more comprehensive report of μSR and magnetization measurements of $Sr_{1-x}Ca_xRuO_3$ by adding (1) the results of $1/T_1$ measurements, performed in longitudinal external field (LF), which revealed diminishing dynamic critical behavior as the phase boundary is approached, (2) comparison of the results on $1/T_1$ with predictions from the SCR theory, (3) new data points of ZF μSR for a few interpolating x values, (4) more detailed analysis on the results for $x = 0.75$, 0.8, 0.9, and 1.0, and (5) ac susceptibility results, which provide severe constraints to the possible spread of the substitution concentration x.

Although magnetization,[24,26,31] structural,[23] NMR,[32–34] Raman,[35] Mössbauer effect, and PAC[36] studies found no evidence for static long-range order in $CaRuO_3$, some controversy remains because earlier reports from Mössbauer effect[37,38] and magnetization[37,38] claim magnetic order in $CaRuO_3$ developing at rather high temperatures as ~90 K, and a theoretical calculation[39] predicts a crossover from ferromagnetic to antiferromagnetic interactions at $x = 0.724$ and subsequent spin-glass state for $CaRuO_3$ with dominant short-range antiferromagnetic interactions. It should also be noted that magnetization studies reported signatures suggestive of canted AFM spin freezing[40] near $x = 0.8$ and spin-glass-like behavior[41] at $x = 0.90$–95. Substitutions of dilute magnetic impurities Ti, Fe, Mn, Ni, and Cr on the Ru site in $CaRuO_3$ result in ferromagnetism,[42–44] while Co substitution induces spin-glass behavior.[45] These results demonstrate that $CaRuO_3$ is very close to a magnetic instability, and its vicinity is sensitive to perturbation.

The present study will also provide clarifications to the controversy of $CaRuO_3$ and elucidate magnetism of systems with small (Ca,Sr) substitutions ($0.75 < x < 1.0$) by showing (a) clear evidence for absence of static magnetic order in $CaRuO_3$ and $Sr_{0.1}Ca_{0.9}RuO_3$ down to $T = 2$ K and (b) new μSR results that indicate a spin freezing with a very small average frozen moment (less than 0.004 Bohr magneton per formula unit) occurring in a small volume fraction in the $x = 0.75$ and 0.80 systems. This paper is organized as follows: we will present sample preparation in Sec. II, magnetization measurements in III, μSR results in IV, and discussions and conclusions in Sec. V.

II. SAMPLE PREPARATION

Polycrystalline samples of $Sr_{1-x}Ca_xRuO_3$ were synthesized by a conventional solid state reaction method. Stoichiometric mixture of powders of $SrCO_3$ (99.99%), $CaCO_3$ (99.99%), and Ru (99.9%) were ground and reacted at 1173 K for 24 h in air. The samples were reground, pressed into pellets, and heated again at 1573 K for 24 h. This procedure was repeated several times, and then the samples were cooled to room temperature at the rate of 1 K/minute in the last procedure.

III. MAGNETIZATION MEASUREMENTS

We performed dc magnetization measurements using a Quantum Design SQUID magnetometer at Columbia University, New York, and ac magnetization measurements at McMaster University, Canada. Figure 1 shows magnetization measurements of the $Sr_{1-x}Ca_xRuO_3$ systems with $x = 0.0$, 0.5, 0.65, and 0.7 in an applied field of (a) 5 G and (b) 1 kG. The vertical arrows show the temperature of the onset of static magnetic order measured using the μSR technique as described later. The magnetization measured under 1 kG is approximately ten times larger than the magnetization measured under 5 G. $Sr_{0.3}Ca_{0.7}RuO_3$ is very weakly ferromagnetic, being the closest to the magnetic/nonmagnetic crossover expected around a calcium concentration $x = 0.7$ and $T = 0$ K. Figure 1(c) shows the ac susceptibility (χ_{ac}) measurements, at a frequency of 1000 Hz and field amplitude of 1 G, in the $x = 0.0$, 0.5, 0.65, and 0.7 systems. For $x = 0.65$ and 0.7, the peaks of χ_{ac} occur at temperatures significantly lower than the onset of static magnetism detected by μSR. In the $x = 0.8$ and 0.9 systems, χ_{ac} increases below 20 K, as shown in Fig. 1(d), without showing a definite peak corresponding to a magnetic transition. The kink observed in $x = 0.9$ is

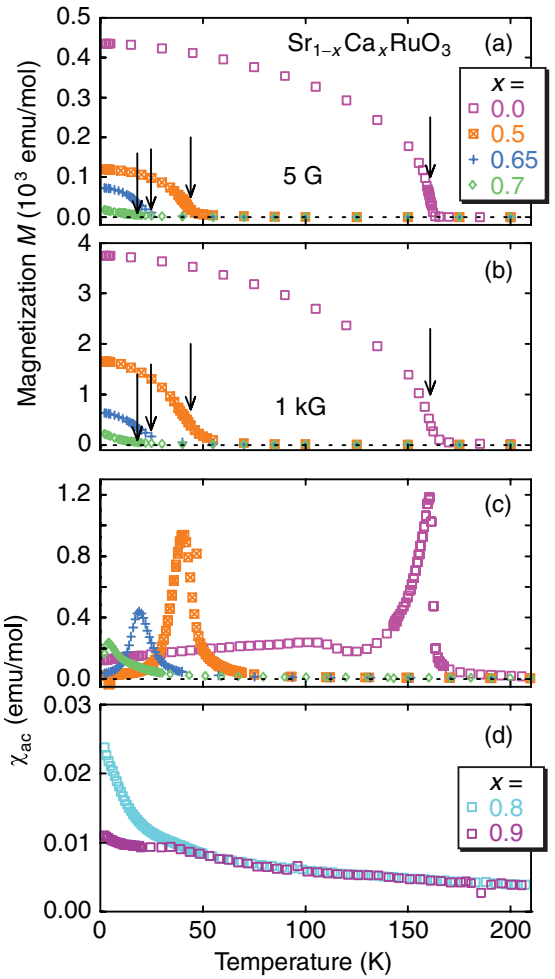

FIG. 1. (Color online) (a) Field-cooled dc magnetization M of $Sr_{1-x}Ca_xRuO_3$ samples with $x = 0.0$, 0.5, 0.65, and 0.7 under an applied field of 5 G. The arrows represent the temperature at which the onset of magnetic order is detected by μSR measurements. (b) Magnetization M under an external magnetic field of 1 kG. (c) ac magnetic susceptibility χ_{ac} of the $x = 0.0$, 0.5, 0.65, and 0.7 systems at frequency of 1000 Hz, and field amplitude of 1 G. (d) ac magnetic susceptibility χ_{ac} of the $x = 0.8$ and 0.9 systems under the same experimental conditions.

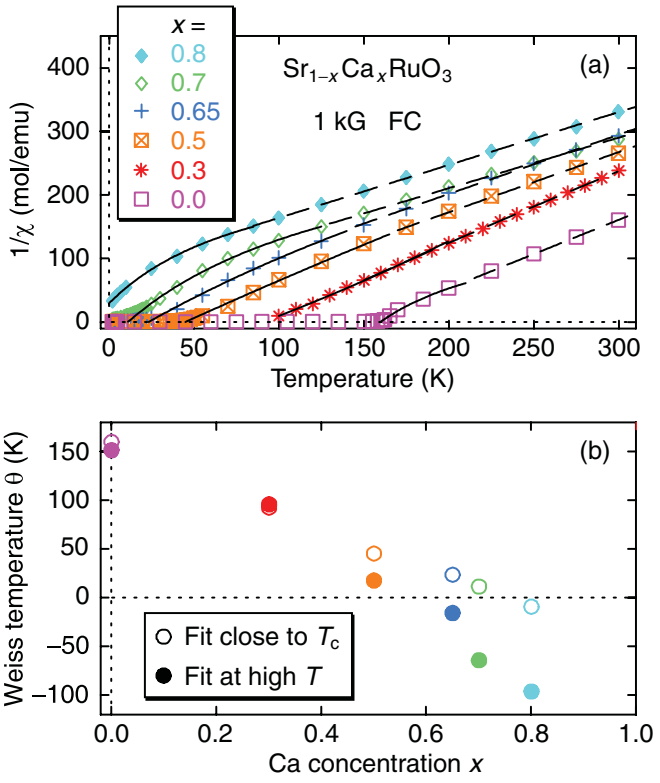

FIG. 2. (Color online) (a) Inverse dc-magnetic susceptibility plotted as a function of temperature for systems with $x = 0.0$, 0.3, 0.5, 0.65, 0.7 and 0.8. The dependence is linear at high temperatures. These results exhibit nearly parallel lines in the plot of $1/\chi$ versus temperature. (b) The Weiss temperature θ determined from a fit of the susceptibility to a Curie-Weiss law. Fitting the data right above the magnetic transition yields θ values close to T_c.

presumably due to a contamination by a tiny ferromagnetic component.

By comparing the widths of the peaks in χ_{ac}, one can estimate the degree of chemical inhomogeneity in the sample. The peak observed in $x = 0.5$ is 1 K wider than the peak of the pure $SrRuO_3$. Assuming that this reflects a variation in T_c due to composition spread, we expect a standard deviation of calcium concentration of ± 0.6 %. The peak of $x = 0.65$ is larger by 1.5 K than the peak of $SrRuO_3$, which leads to a chemical composition spread of about 1.2 %. Thus we expect the composition variation in the samples to be less than $\sim$1 % in the present specimens.

Figure 2(a) shows the inverse dc-magnetic susceptibility $1/\chi$ as a function of temperature under an applied magnetic field of 1 kG for $x = 0.0$, 0.3, 0.5, 0.65, 0.7, and 0.8. The plots become linear at high temperatures, where a Curie-Weiss-like behavior of the susceptibility is expected for magnetic systems with itinerant electrons. Figure 2(b) shows the Weiss temperature θ determined by fitting the susceptibility with a Curie-Weiss law. Two results were obtained for each sample: one from the fit in the high-temperature (high-T) range and the other in the low-temperature (low-T) range (fitting temperature ranges for each specimen is given in Ref. 46). A constant term was added to the latter fit. For systems with $x \geqslant 0.5$, θ derived from the high-T data is significantly smaller (or more negative) than θ obtained from the low-T data. For ferromagnetic systems, the low-T fits yield θ values close to T_c.

IV. μSR MEASUREMENTS

A. Experimental details

We performed zero-field (ZF) μSR measurements at the M20 Channel of TRIUMF, Vancouver, Canada. In a time differential experiment, positive muons, polarized along the flight direction, are implanted one at a time in the sample. Within less than a nanosecond, the muon stops at the location(s) of minimum electrostatic potential energy within the unit cell. The muon spin then changes orientation as it interacts with the local static or fluctuating magnetic fields. The muon subsequently decays into a positron and two neutrinos (the muon lifetime is 2.2 μs) and due to parity violation in muon decay, the positron is emitted preferentially along the muon spin direction. For all experiments, we used a muon

beam with momentum of ~ 28MeV/c. The samples were made in pressed pellets of approximately 1 cm in diameter and 2 mm thickness. The largest surface was placed perpendicular to the beam direction.

In zero-field (ZF) or longitudinal field (LF) configurations, the positrons are detected by forward and backward counters placed along the direction of the beam, commonly labeled the z direction. The sample is located between the two detectors. Histograms of the positrons from muon decay events are recorded as a function of the time t, which represents the residence time of the muons in the crystal between the implantation and decay. The statistical average of the projection of the muon spin on the z axis, $P_\mu^z(t)$, is obtained from the two time histograms as a function of t. At $t = 0$, $P_\mu^z(t) = 1$ since initial muons spins point in one (backward) direction. At longer times, when the muon spin orientation is randomized and there is no longer any difference between the average number of positron counts registered in the forward and the backward counters, $P_\mu^z(t)$ becomes 0. The amplitude of the μSR signal is denoted as the asymmetry and the time-dependent asymmetry is given by the muon polarization function multiplied by the initial asymmetry of the signal.

B. Fitting function for the time-dependent muon spin polarization

Figure 3 shows the muon spin polarization $P_\mu^z(t)$ at several temperatures, observed in the systems with $x = 0.0$, 0.3, 0.5, 0.65, 0.7, 0.75, 0.8, 0.9, and 1.0. Fast depolarization is observed at low temperatures in $x = 0.0$, 0.3, 0.5, 0.65, and 0.7, indicating that the local fields in these systems are strong and static magnetic order is achieved. The spin fluctuations slow down near $T = T_c$, causing faster depolarization of the muon spin around T_c than at high temperatures, as can be seen by comparing the top and the middle plots for each ferromagnetic sample. The $x = 0.75$ and 0.8 compounds also show an increase of muon spin depolarization at low temperatures. As we describe later in the paper, additional LF measurements, with external magnetic fields applied along the initial direction of the muon spin, enable us to show that the depolarization in the $x = 0.75$ and 0.8 systems is caused by very small static fields (3–4 G). There is no difference between the low-temperature and the high-temperature muon spin polarization in $CaRuO_3$, indicating that the sample is paramagnetic above $T = 2$ K.

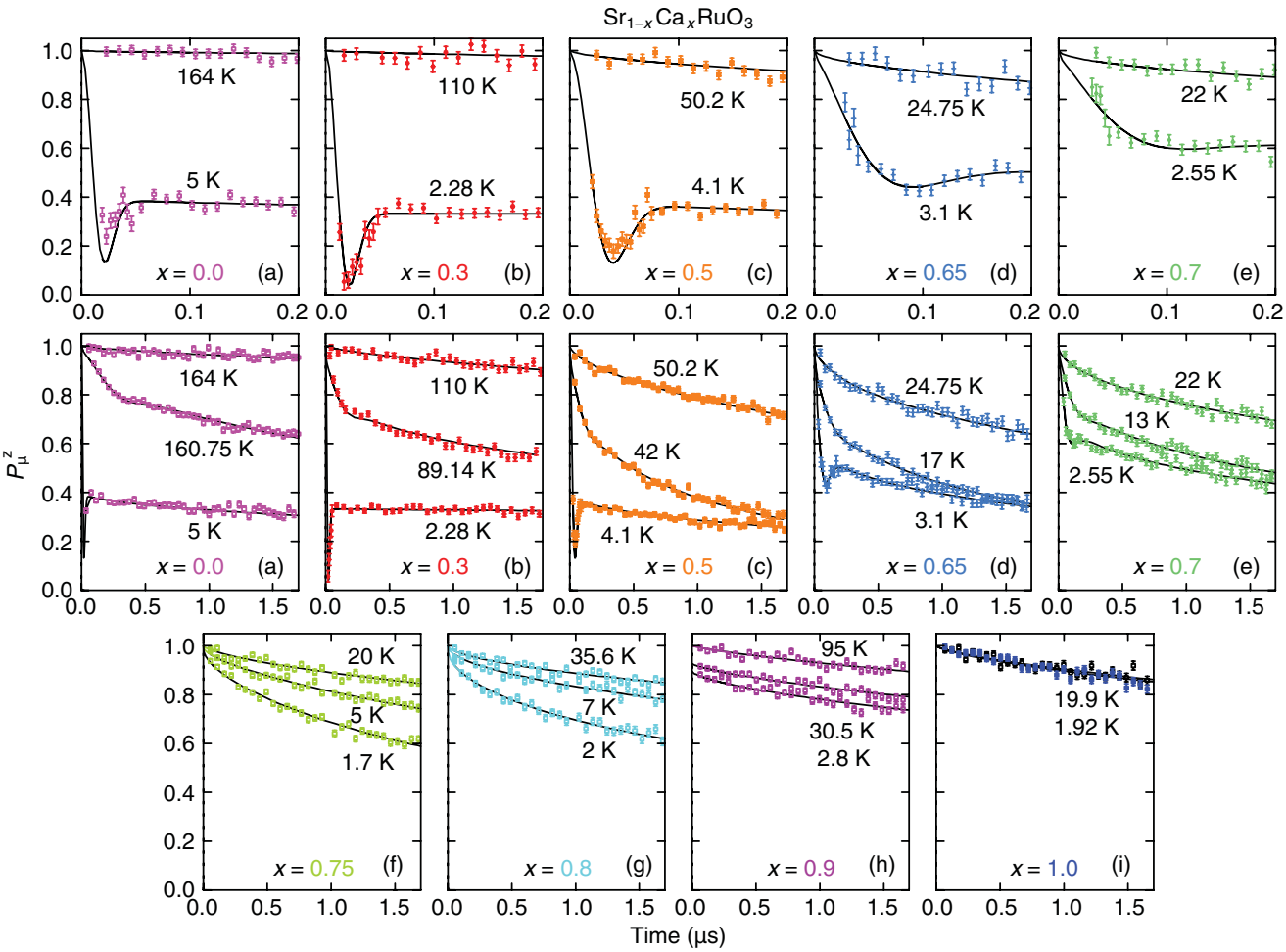

FIG. 3. (Color online) Time spectra of the muon spin-polarization function, P_μ^z, observed in zero field in $Sr_{1-x}Ca_xRuO_3$ with $x = 0.0$, 0.3, 0.5, 0.65, 0.7, 0.75, 0.8, 0.9, and 1.0 at a few representative temperatures. The top row figures show early-time regions of the middle row figures.

The $x = 0.0$, 0.3, and 0.5 systems exhibit static magnetic order in the entire volume at low temperatures. This can be seen from the amplitude (2/3) of the fast damped oscillation of $P_\mu^z(t)$ at early time, shown in the top row of Fig. 3. The damped oscillation is followed by a slowly relaxing 1/3 component. In the $x = 0.65$ and 0.7 systems, the amplitude of the damped oscillation is less than 2/3, which is an indication that only a fraction of the sample volume undergoes static magnetic order.

In the paramagnetic state of ferro- or antiferromagnets, the muon spin polarization function is determined by static nuclear dipolar fields and fluctuating dynamic fields from electron spins. For systems with rapid electron spin fluctuations, the two contributions are independent and $P_\mu^z(t)$ can be given as their product. In the present study, the dynamic relaxation due to electron spins was fitted to $\exp[-(\lambda t)^\beta]$, with $0.33 < \beta < 1.0$. β is determined by inhomogeneity in the system, with β smaller for less homogeneous systems.[48,49] For systems with a unique value of local field at the muon sites, one would expect $\beta = 1$, corresponding to the $1/T_1$ exponential relaxation with a single slope. The values of β, obtained from the present data as a free fit parameter, were about 0.5–0.6 for most of the systems in a wide temperature range. This is presumably related to a significant spread of the instantaneous local field as discussed later.

The very weak nuclear dipolar field in the $Sr_{1-x}Ca_xRuO_3$ samples is generated by the (nuclear) magnetic isotopes of Sr, Ca, Ru, and O. They form a dilute system of moments, whose contribution to the muon spin polarization function is of the form $\exp(-\lambda_{dip}t)$. The relaxation rate λ_{dip}, proportional to the magnetic moment/unit cell, can be estimated by comparing the magnetic moment/unit cell of the present systems with the results in a dilute-alloy spin glass CuMn (1 at.% Mn).[48] This calculation yields λ_{dip} in the range $5.5–7.5 \times 10^{-3}$ μs^{-1} for the present systems.

Well above T_c, the relaxation due to fluctuating electronic spins is small and the nuclear dipolar fields dominate the muon spin relaxation process. Application of a small longitudinal magnetic field of 100 G "decouples" the nuclear dipolar fields, making their contribution to P_μ^z negligible. Therefore, comparison of the ZF and LF spectra at high temperatures allows to estimate an upper limit for λ_{dip}. We found $\lambda_{dip} = 1 \times 10^{-2}$ μs^{-1}, consistent with the evaluations above. We used this value in the analysis of the data for all samples. This is an extremely slow relaxation, so in practice the effect of nuclear dipolar field is negligible in the present study.

In the magnetically ordered phase, the relaxation due to the nuclear dipolar fields is much smaller compared to the effect of static internal fields from the spontaneously ordered Ru moments. P_μ^z is then given as a product of a Kubo-Toyabe function, describing the muon depolarization due to static fields from the frozen component of electron spins, and $\exp[-(\lambda t)^\beta]$, which accounts for the effect of dynamic electron spins.

In the absence of an external applied magnetic field, the Kubo-Toyabe function is given as

$$G_z(t) = \frac{1}{3} + \frac{2}{3}(1 - \Delta^p t^p)\exp\left(-\frac{\Delta^p t^p}{p}\right), \qquad (1)$$

where Δ is proportional to the root mean square width of distribution of magnetic fields probed by the muons, and $1 \leqslant p \leqslant 2$. In the limiting case with $p = 2$, one obtains the Gaussian Kubo-Toyabe function $G_z^{GKT}(t)$,[47] which is appropriate for systems with randomly oriented, dense, static spin systems. In these systems, the distance between local moments is approximately the same as the distance between the muon and the magnetic moments. Each muon will experience magnetic fields from the same Gaussian distribution of local fields. The function with $p = 1$ in Eq. (1) describes the systems with dilute moments, where the muon will experience stronger or weaker field distributions, depending on how far the muon site is from a magnetic moment. Overall, the distribution of magnetic fields probed by the muon is Lorentzian.[48] Cases intermediate between the dense and dilute spin systems could be investigated by varying the parameter p in the interval $1 < p < 2$. We obtained the values of p by fitting data observed at low temperatures, as $p = 2.0$, 2.0, 1.61, 1.57, 1.0 and 1.0, respectively, for the systems with $x = 0.3$, 0.5, 0.65, 0.7, 0.75, and 0.8, and kept these values fixed for higher temperatures. For $SrRuO_3$ ($x = 0$), we adopted $p = 2.0$ in data analyses for the purpose of comparisons with adjacent $x = 0.3$ and 0.5 systems, while a more detailed internal field profile will be described later.

In the present systems, the magnetic ordering takes place in a rather broad temperature interval. The volume fraction V_f of the sample that is magnetically ordered, $0 < V_f < 1$, increases monotonically as the temperature is decreased through T_c. Therefore all the data have been fit using the function

$$P_\mu^z(t) = [V_f G_z(t) + (1 - V_f)\exp(-\lambda_{dip}t)]\exp[-(\lambda t)^\beta]. \qquad (2)$$

C. μSR results for the ferromagnetic systems with $x = 0.0$, 0.3, 0.5, 0.65 and 0.7

Figure 4(a) shows the temperature dependence of the root mean square width Δ of the distribution of local fields probed by the muon. Δ was converted from μs^{-1} to kG using the gyromagnetic ratio of the muon spin, $\gamma_\mu = 2\pi \times 13.554$ MHz/kG. Ferromagnetic order appears below 160.75 K, 92.1 K, 44 K, 24.7 K, and 18 K in the systems with $x = 0.0$, 0.3, 0.5, 0.65, and 0.7, respectively. In each system, the local field monotonically increases as the temperature decreases.

The volume fraction V_f of regions with static magnetic order is shown in Fig. 4(b) for the ferromagnetic systems. As the temperature is decreased, static magnetic order in full volume is achieved only in $SrRuO_3$, $Sr_{0.7}Ca_{0.3}RuO_3$, and $Sr_{0.5}Ca_{0.5}RuO_3$, which have strong magnetism with high Curie temperatures and large ordered moments. The fraction V_f changes from 0 to 1 over a temperature interval of approximately 23 (could be affected by poor early-time resolution), 12 and 15 K, respectively, in the $x = 0.0$, 0.3, and 0.5 systems. This represents 14%, 13%, and 34%, respectively, from the temperature at which the onset of magnetism is observed. In $Sr_{0.35}Ca_{0.65}RuO_3$ and $Sr_{0.3}Ca_{0.7}RuO_3$, the proportion of the ordered phase increases slowly as the temperature is decreased, reaching values in the range of $59 \pm 3\%$ and $34 \pm 2\%$ at $T = 2$ K.

The product of the local field width Δ and the ordered volume fraction V_f is shown as a function of temperature in Fig. 4(c), expressed in units of Bohr magneton per atom

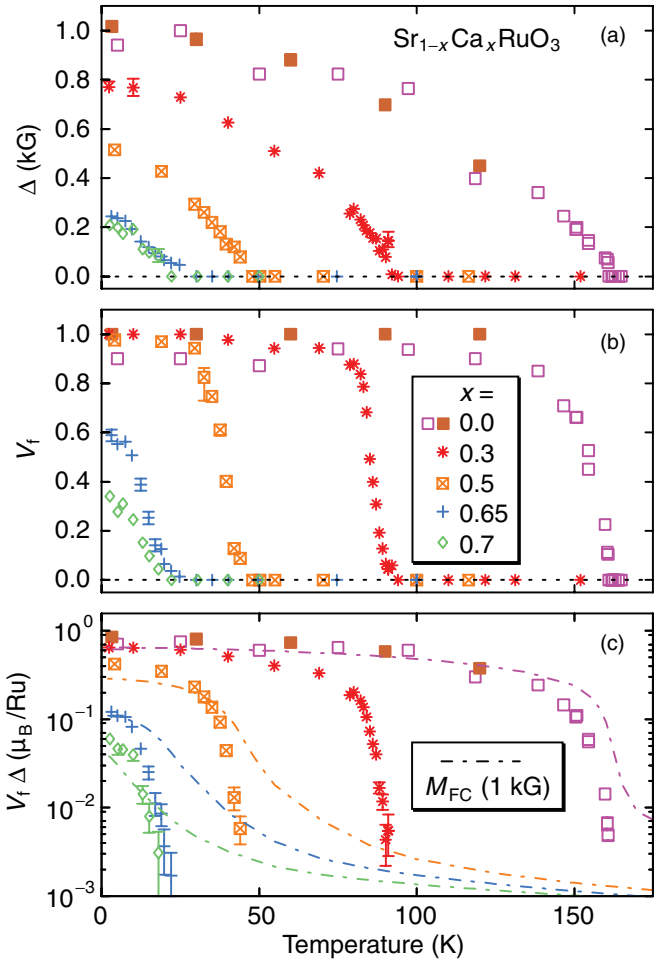

FIG. 4. (Color online) (a) The width of the static local field, Δ (kG), determined by ZF μSR, shown as a function of temperature for the ferromagnetic $Sr_{1-x}Ca_xRuO_3$ with $x = 0.0$, 0.3, 0.5, 0.65, and 0.7. The symbols are labeled in panel (b). (b) The temperature dependence of the volume fraction V_f of regions with static magnetic order. The $x = 0.0$, 0.3, and 0.5 systems achieve static magnetic order in the entire volume, while the $x = 0.65$ and 0.7 systems exhibit static order only in a partial volume fraction even at $T \to 0$. (c) The data points denote the product of the local field width and the ordered volume fraction $V_f\Delta$ derived from ZF μSR and expressed in units of Bohr magneton/atom. The dashed lines represent the magnetic moment/atom derived from the FC magnetization measurements under 1 kG. The two measurements agree reasonably well at low temperatures.

using calibration obtained from the results of $SrRuO_3$. At low temperatures, $V_f\Delta$ agrees with the magnetic moment/atom derived from field-cooled dc-magnetization measurements under 1 kG, M_{FC} (dashed line). As described later, M_{FC} in this condition is approximately equal to the spontaneous magnetic moment/atom. For systems that have magnetic order only in a partial volume fraction, the bulk magnetization should correspond to the product of the local magnetic field Δ and the volume fraction V_f.

The behaviors of the field width and the volume fraction at the limit of low temperatures ($T \to 0$) are shown in Fig. 5 as a function of the calcium concentration x. The $x = 0.0$, 0.3, 0.5, 0.65, and 0.7 systems are ferromagnetic. As presented in detail

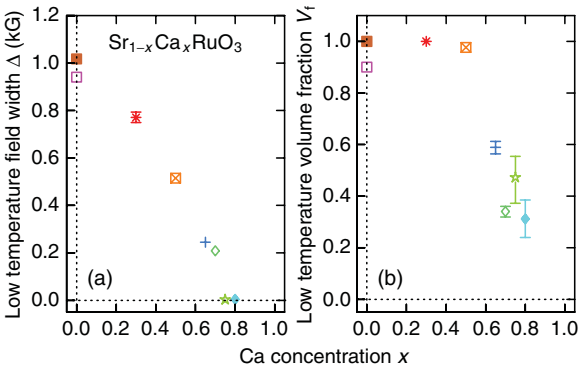

FIG. 5. (Color online) (a) The width Δ of the distribution of static local magnetic fields, plotted as a function of calcium concentration x for $Sr_{1-x}Ca_xRuO_3$ with $x = 0.0, 0.3, 0.5, 0.65$, and 0.7. The green star and the blue diamond show the very small rms field widths found in $Sr_{0.25}Ca_{0.75}RuO_3$ and $Sr_{0.2}Ca_{0.8}RuO_3$, as discussed in the text. (b) The volume fraction V_f of regions with static magnetic order at $T \to 0$, plotted against Ca concentration x. Only the samples with $x = 0.0$, 0.3, and 0.5 achieve static magnetic order in the entire volume.

later, an extremely small static magnetic field of the order of a few Gauss was found in $x = 0.75$ and 0.8. Figure 5(a) demonstrates a drastic reduction of the static field width in $x = 0.75$ and 0.8 from that in the ferromagnetic $x = 0.7$ and 0.65 systems. This suggests a different type of magnetism in the compounds with $x = 0.75$ and 0.8. Figure 5(b) shows the volume fraction of regions with static magnetism at the limit of low temperatures. The data indicates phase separation between magnetic and paramagnetic regions in the weakly ferromagnetic samples with $x = 0.65$ and 0.7. There is phase separation between regions with and without static order also in the $x = 0.75$ and 0.8 systems. The large error bars in their case are due to large tradeoffs between parameters of the fit.

In Fig. 6, we compare (1) the low-temperature local field width times the ordered volume fraction $V_f\Delta$ determined by μSR, (2) the low-temperature spontaneous moment p_s, and (3) the low-temperature dc magnetization M_{FC} obtained from field-cooled measurements under 1 kG. The spontaneous moment was determined by reducing the magnetic field to 0 after the sample was magnetized under 5 T. The inset on the right-hand side shows part of the hysteresis loop for $SrRuO_3$ and p_s is indicated by an arrow. Magnetic systems with itinerant electrons generally exhibit significant high-field magnetic susceptibility. The magnetization M observed in the inset still increases with increasing B even at high magnetic fields such as 5 T, which is the limit of our SQUID magnetometer. All three results (1)–(3) exhibit very good quantitative agreement. For all the systems, M_{FC} is comparable to p_s. The effective paramagnetic moment per atom determined from the Curie constant is shown at the top panel of Fig. 6 for comparison. In all samples, p_{eff} is much larger than p_s, as expected for ferromagnetic systems based on itinerant electrons.

D. μSR time spectra of $SrRuO_3$

In $SrRuO_3$, a second set of data with better early-time resolution have been taken to accurately determine the field

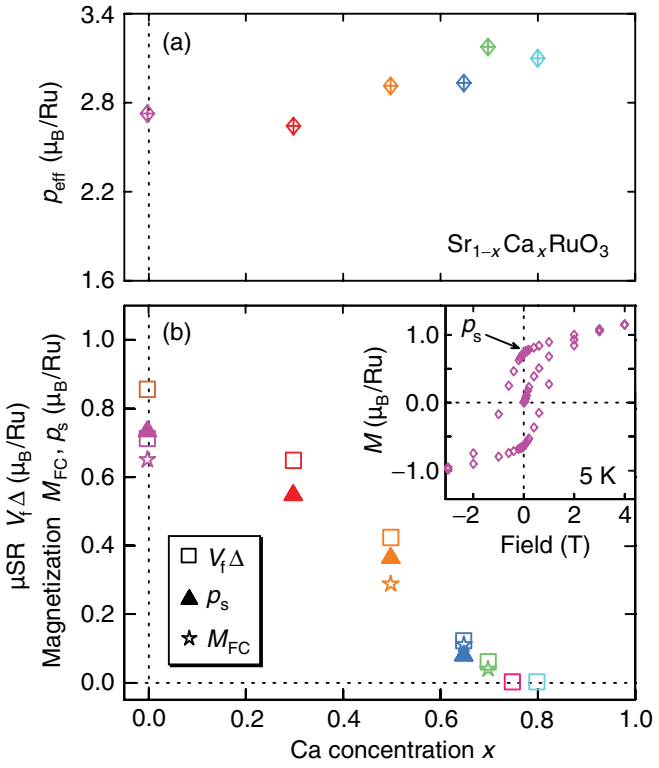

FIG. 6. (Color online) Comparison of the ordered volume fraction times the local field width $V_f\Delta$ determined by μSR, the low-temperature magnetic moment p_s, and the low-temperature magnetization M_{FC} obtained from field-cooled measurements under 1 kG. The results for these three parameters show good agreement. The inset shows the spontaneous moment of the $SrRuO_3$ obtained from the hysteresis loop. The upper panel shows the effective paramagnetic moment p_{eff} determined from the Curie constant after fitting the inverse susceptibility $1/\chi$ at high temperatures.

amplitude at low temperatures. The resulting time spectra in ZF are shown in Fig. 7, which exhibits a distinct oscillation observed below T_c. The observation of a highly damped oscillatory signal is consistent with the recent results of Blundell *et al.*.[50] These spectra can be fitted to the two-frequency function

$$A_0 P_\mu^z(t) = a_1 \exp(-\lambda_1 t)\cos(2\pi\nu_1 t + \phi) + a_2 \exp(-\lambda_2 t)\cos(2\pi\nu_2 t + \phi) + a_3, \quad (3)$$

where A_0 is the asymmetry at $t = 0$, λ_1, and λ_2 are the damping rate of the oscillation, and ν_1 and ν_2 are the muon precession frequencies. The temperature dependence of ν_1 and ν_2 is shown in the inset of Fig. 7. The two different frequencies can be attributed to two magnetically inequivalent muon sites. Probabilities of muons to occupy these sites, $a_1/(a_1 + a_2)$ and $a_2/(a_1 + a_2)$, are comparable to each other. The nonoscillating component $a_3 \sim A_0/3$ represents muons stopped at sites where the internal field is parallel to the initial muon polarization.

The large values $\sim 40\ \mu s^{-1}$ of the damping factors λ_1 and λ_2 indicate a broad distribution of the internal magnetic field. This may be due to further variation of muon sites, plus other possible factors including grain boundaries and shape-dependent demagnetizing fields in ferromagnets. The

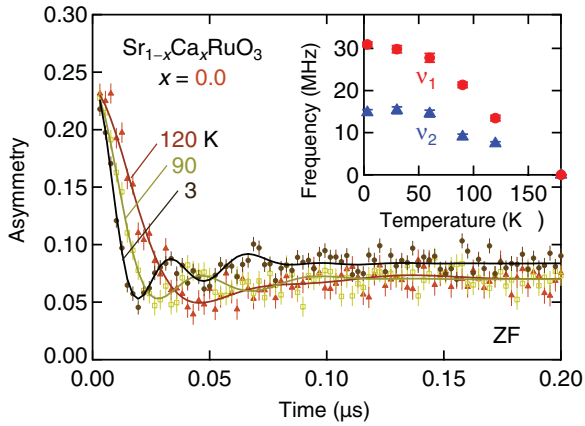

FIG. 7. (Color online) ZF-μSR time spectra observed in $SrRuO_3$ ($x = 0.0$). The solid lines represent fits to the data with the two-frequency function (1). The inset shows temperature dependence of muon precession frequencies ν_1 and ν_2.

wide distribution of internal fields, resulting from the multiple muon sites, is consistent with a small value of $\beta \sim 0.5$ observed in the paramagnetic state. When the time spectra of Fig. 7 are fit using Eq. (1) with p as a free parameter, we obtain $p \sim 1.5$. The average field strength Δ for this value of p (not shown in the graph) agrees within $\pm 10\%$ with the Δ values obtained for $p = 2.0$ shown with closed square symbols in Figs. 4–5. No precession frequency was resolved in ZF-μSR spectra of other systems.

E. μSR studies of the $Sr_{0.2}Ca_{0.8}RuO_3$ and $Sr_{0.25}Ca_{0.75}RuO_3$ systems

High-field magnetization measurements of polycrystalline samples up to 44 T indicated that $Sr_{0.2}Ca_{0.8}RuO_3$ is an exchange enhanced paramagnet on the verge of static magnetism.[24] The system shows large increase of magnetization in external field at low temperature and large value of the high-field susceptibility, as expected in the case of nearly ferromagnetic systems.

Figure 8(a) shows the time-dependent muon spin polarization function P_μ^z in $Sr_{0.2}Ca_{0.8}RuO_3$ at $T = 2$ K under zero

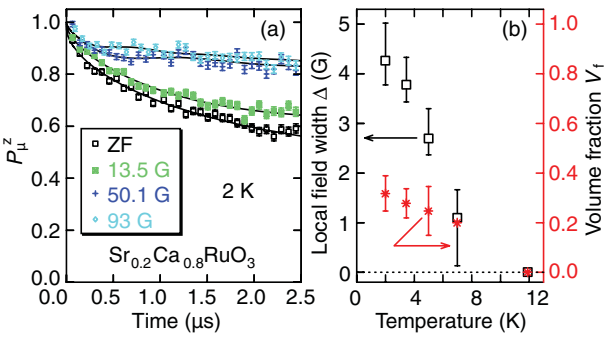

FIG. 8. (Color online) (a) Time spectra of muon spin polarization function in $Sr_{0.2}Ca_{0.8}RuO_3$ under zero field and longitudinal fields of 13.5, 50.1, and 93 G at $T = 2$ K. (b) The width of the local field distribution Δ (black open squares) and the volume fraction with static magnetic order V_f (red stars) plotted as a function of temperature. Static fields persist in the sample up to at least 7 K.

field and longitudinal magnetic fields of 13.5, 50.1, and 93 G applied along the direction of the initial muon polarization. The data were fit in the range from 0.035 to 8.0 μs assuming partial magnetic order in the sample. Under ZF conditions, the contribution to the fit function from magnetically frozen regions is in the form of a Lorentzian function, i.e., Eq. (1) with $p = 1$. The contribution of electronic spin fluctuation is in the form of a stretched exponential as shown in Eq. (2). At 2 K, the volume fraction of the sample that is magnetically ordered is $32 \pm 7\%$ and the width of the distribution of local fields is 4.3 ± 0.8 G. Since the data taken under a longitudinal field (LF) of 93 G is similar to data under 50.1 G, a magnetic field of about 93 G is sufficient to "decouple" the contribution of static fields from that due to electronic spin fluctuations. The relaxation at 50.1 and 93 G are due primarily to electron spin fluctuations. The width of distribution of local fields derived from LF data is consistent with those from the ZF data. Figure 8(b) shows the temperature dependence of the volume fraction V_f and the width Δ derived from ZF-μSR data. The static field decreases monotonically as temperature is increased and vanishes somewhere between 7 and 12 K. The ordered fraction was a free fit parameter at all temperatures except at 7 K where it was set to 20% to be able to fit the data. The ordered fraction also appears to decrease with increasing temperature.

The μSR measurements are consistent with our FC magnetization measurements performed under magnetic fields of 5, 100, and 1000 G. The magnetization increases significantly below ~20 K. At high temperatures the magnetic susceptibility is Curie-Weiss-like and $1/\chi$ is linear in T as shown in Fig. 2(a). We also found a small amount of hysteresis in the $Sr_{0.20}Ca_{0.80}RuO_3$ sample, persisting up to ~20 K.

We performed a similar μSR study for $Sr_{0.25}Ca_{0.75}RuO_3$. The data analysis is the same as for the $Sr_{0.2}Ca_{0.8}RuO_3$, except that at each temperature the ZF and LF data were fit simultaneously to determine the small magnetic field in the sample. At $T = 1.7$ K, the volume fraction V_f is around $50 \pm 10\%$ and the width of the distribution of local fields is $3.0 \pm 0.4\%$ G. Figure 9(a) shows the muon polarization function P_μ^z at 1.7 K under ZF and LF of 24.9, 48.9, and 100 G. As in the $x = 0.8$ system, a magnetic field of 100 G is sufficient to "decouple" the relaxation due to static fields.

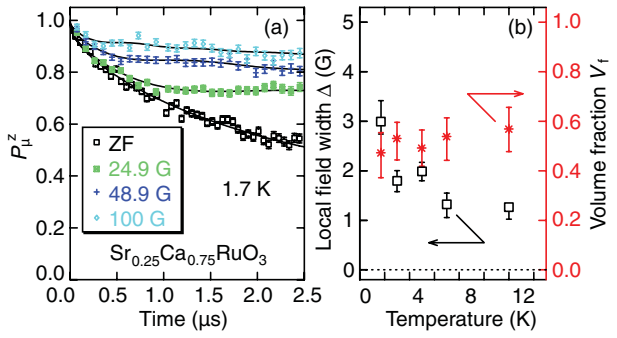

FIG. 9. (Color online) (a) Time spectra of muon spin polarization function in $Sr_{0.25}Ca_{0.75}RuO_3$ under zero field and longitudinal fields of 24.9, 48.9, and 100 G. (b) The width of the local field distribution Δ (black open squares) and the volume fraction of the sample that is magnetic V_f (red stars). Static fields appear to persist in the sample up to at least 12 K.

Figure 9(b) shows the ordered fraction V_f and the local field width Δ as a function of temperature. Static local fields persist up to about 12 K.

Our μSR measurements are not conclusive about the spatial spin correlations in $Sr_{0.2}Ca_{0.8}RuO_3$ and $Sr_{0.25}Ca_{0.75}RuO_3$. It should be stressed, however, that the size of the ordered moment of 0.004 Bohr magneton per Ru, obtained by scaling the results of ferromagnetic $SrRuO_3$ (0.8 Bohr magneton per Ru) with the observed local field width, is extremely small in systems with $x = 0.75$ and 0.8. Thus the mechanism for magnetic order of these systems could be very different from the rather standard ferromagnetic order for $x \geqslant 0.7$. The very slow initial exponential decay, due to static magnetism, is suggestive of a freezing of very dilute moments with the concentration of the order of 100 to 1000 ppm per unit cell.

F. μSR measurements of the dynamic spin relaxation rate $1/T_1$

The present study on $Sr_{1-x}Ca_xRuO_3$ is a part of a series of μSR studies of the critical behavior of itinerant ferromagnets. The first experiments performed by Hayano *et al.*[51] on the weakly itinerant helimagnet MnSi ($T_c = 29.5$ K) revealed critical divergence of the spin-lattice relaxation rate measured under an applied field of LF = 700 G. A linear dependence was found when the relaxation time T_1 was plotted as a function of $1/T$, in agreement with the SCR theory of spin fluctuations.[13] In a more recent μSR study of MnSi, we found an LF dependence of the relaxation rate $1/T_1$ in the paramagnetic state.[52] The field dependence, persisting up to 2.7 kG, is due to the helical/conical spin structures specific to MnSi, where the remaining helical component of the spin fluctuations perpendicular to the LF selectively contribute to the relaxation.

In order to make universal treatments of the dynamic effects for spectra fitted with different power β of the power exponential decay, in this paper, we define the muon spin relaxation time T_1 as the time required for the muon spin polarization due to fluctuating electronic spins, $\exp[-(\lambda t)^\beta]$, to become half of the value at $t = 0$, i.e.,

$$T_1 = \frac{[\ln(2)]^{1/\beta}}{\lambda}. \tag{4}$$

The parameter β was treated as a free fit parameter, and was less than 1 around T_c. Figure 10(a) shows the relaxation rate $1/T_1$ observed in ZF and/or low LF below 100 G, as a function of temperature. The peak temperature of the $1/T_1$ versus T plot was chosen as the critical temperature T_c. The relaxation rate takes maximum values around $T = 154.5$, 85.0, 37.6, 14.8, and 13.0 K for the $x = 0.0$, 0.3, 0.5, 0.65, and 0.7 systems, respectively. These peak temperatures are well within the temperature interval of the magnetic transition estimated from V_f, and are approximately in the center of the interval for the samples with $x = 0.3$ and 0.5.

In Fig. 10(b), we plot the relaxation time T_1 as a function of the inverse temperature $1/T$. In the paramagnetic state of the $x = 0.0$, 0.3, 0.5 and 0.65 systems, T_1 shows an approximate linear dependence on $1/T$. For the $x = 0.0$ and 0.3 systems, the linearity can be seen only close to T_c. Further away from T_c the relaxation rates due to electron spin fluctuations and

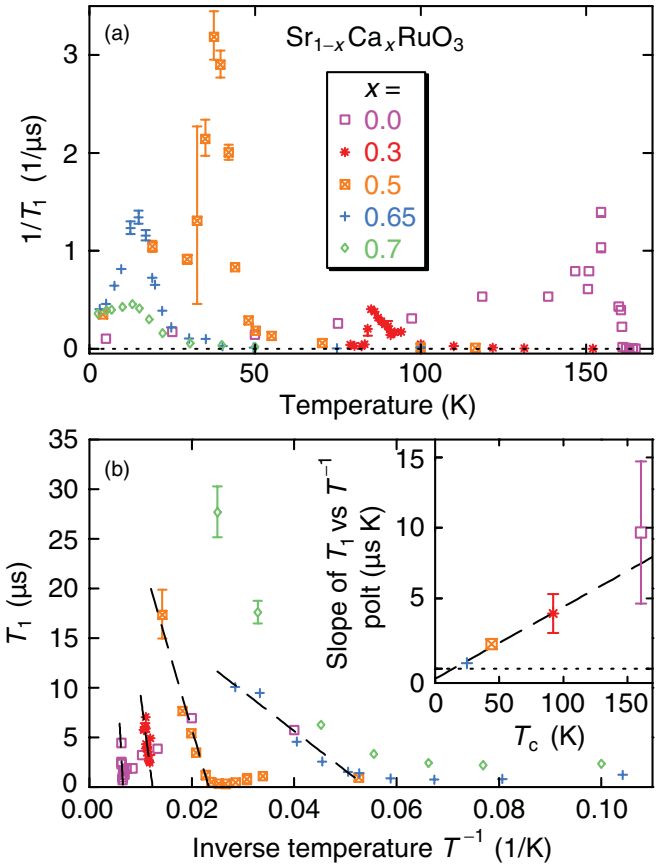

FIG. 10. (Color online) (a) Temperature dependence of the relaxation rate $1/T_1$ for the ferromagnetic samples of $Sr_{1-x}Ca_xRuO_3$. (b) The relaxation time T_1 has a linear dependence on $1/T$ in the paramagnetic phase of the $x = 0.0$, 0.3, 0.5, and 0.65 systems. The data for $x = 0.7$ is spread over a range of $1/T_1$ values and does not confirm this trend. The inset shows the slope of the T_1 vs $1/T$ plot as a function of T_c.

nuclear dipolar fields become comparable, which prevents accurate derivation of the T_1 values.

V. DISCUSSIONS AND CONCLUSIONS

A. Comparison with the SCR theory

The magnetization data in Sec. III agree well with the SCR theory of spin fluctuations of Moriya.[13] According to this theory, the magnetic susceptibility of systems with itinerant electrons is a complex function of temperature, which simplifies to a Curie-Weiss-like law above T_c, but not too close to T_c. The Curie-Weiss-like behavior in itinerant systems is due to the approximately linear increase with temperature of the mean-square local amplitude of thermal spin fluctuations, rather than to fluctuating local moments. In agreement with the SCR theory, the slopes of the $1/\chi$ versus T plots in Fig. 2 are nearly parallel. The Weiss temperatures of the $Sr_{0.2}Ca_{0.8}RuO_3$ is negative, which implies that the system is an exchange-enhanced paramagnet in the framework of the SCR theory. We derived the effective paramagnetic moment $p_{\rm eff}$ from the Curie constant obtained by fitting the high-T inverse susceptibility (dashed line in Fig. 2). The results, shown at the top of Fig. 6, are consistent with those reported in earlier studies.[11,26,38,41]

The present results on $1/T_1$ are also consistent with the SCR theory in which the muon spin relaxation time T_1 is related to the uniform susceptibility χ in the following way:

$$\frac{1}{T_1} = \frac{\hbar\gamma_\mu^2 A_{\rm hf}^2}{2\pi T_{\rm A}} \frac{3t_{\rm rd}}{2y}, \tag{5}$$

where $y = 1/(2T_{\rm A}\chi)$ is the reduced inverse susceptibility, $t_{\rm rd} = T/T_0$ is the reduced temperature, and $A_{\rm hf}$ is the muon hyperfine coupling constant. T_0 and $T_{\rm A}$ are temperatures that characterize the energy width of the dynamical spin fluctuation spectrum and the width of the distribution of static susceptibility in q space. A large T_0/T_c ratio is expected for magnets with itinerant electrons. $T_0 = 234$ K was determined for the $Sr_{0.4}Ca_{0.6}RuO_3$ sample with $T_c = 25$ K,[23] which yields $T_0/T_c \sim 9.4$. In the temperature region where χ obeys a Curie-Weiss law, T_1T depends linearly on $(T - T_c)$. This implies a linear relationship when T_1 is plotted against $1/T$, as shown by our data for the $x = 0.0$, 0.3, 0.5, and 0.65 systems.

The plot of T_1 versus $1/T$ for $Sr_{0.3}Ca_{0.7}RuO_3$ deviates from the linear trend observed for the other ferromagnetic samples. Ishigaki and Moriya[53] showed that T_1 diverges as $T^{-1/3}$ at the magnetic instability in metals. Among the ferromagnetic systems in the present study, the $x = 0.7$ system is the closest to the magnetic crossover. This could explain why the T_1 versus $1/T$ plot is nonlinear, but the critical temperature of the sample is rather large (around 13 K) and our data are insufficient to show the divergence of T_1 as $T^{-1/3}$. Also, calculations we performed for a hypothetical sample that orders over a temperature interval centered on T_c suggest that the curving of the T_1 versus $1/T$ plot could be due also to the broadening of the temperature interval of the magnetic transition, which is very pronounced in the $x = 0.7$ system.

The inset of Fig. 10(b) shows the slopes of the T_1 versus $1/T$ plots as a function of T_c for the $x = 0.0$, 0.3, 0.5, and 0.65 systems. The SCR theory predicts a linear dependence of the slope on T_c. The proportionality can be derived theoretically from Eq. (5) assuming a Curie-Weiss law for the uniform susceptibility. The present data follow the linearity rather well. As shown previously, the broadening of the transition could cause the reduction of the slope for $x = 0.65$, which could make the linear fit of the data points in the inset pass below the origin.

B. Behavior indicating first-order transitions

The present results are summarized in Fig. 11, which shows a phase diagram for the $Sr_{1-x}Ca_xRuO_3$. The critical temperature was derived from μSR measurements for each sample and is plotted with closed squares as a function of calcium concentration x. The systems with $x = 0.0$, 0.3, 0.5, 0.65, and 0.7 are ferromagnets with itinerant electrons, consistent with numerous other measurements. The stripe coloring indicates phase separation between regions with and without static magnetic order. The systems with $x = 0.75$ and 0.8 show an extremely small static field of approximately 3–4 G at low temperatures, but the spatial spin structure can not be determined by μSR. The $x = 0.9$ system was contaminated by a small amount of ferromagnetic phase,

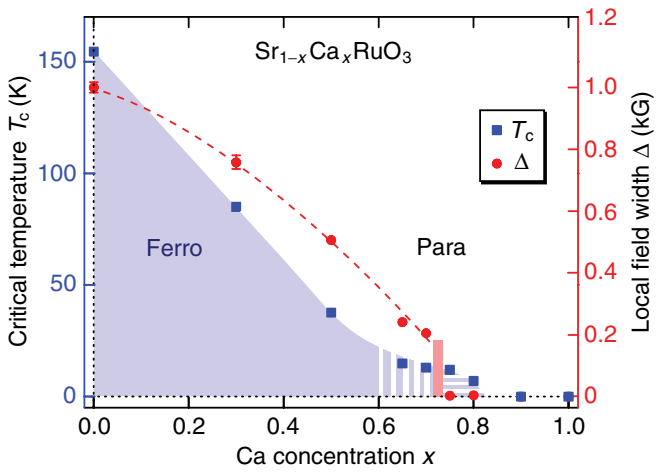

FIG. 11. (Color online) Magnetic phase diagram of the $Sr_{1-x}Ca_xRuO_3$. The critical temperatures (closed squares) are derived from μSR measurements. The red symbols (closed circles) show the local field width in each sample detected by μSR. The systems with $x = 0.0, 0.3, 0.5, 0.65$, and 0.7 are itinerant ferromagnets. The stripe coloring indicates phase separation between regions with and without static magnetic order. The systems with $x = 0.75$ and 0.8 exhibit static order with extremely small moment size in partial volume fraction, but the spatial spin structure cannot be determined by μSR. A transition from ferromagnetic to antiferromagnetic correlations was predicted theoretically at calcium concentration $x = 0.724$.[39] The systems with $x = 0.9$ and 1.0 remain paramagnetic to $T = 2$ K.

but there was essentially no difference between the late-time muon spin relaxation rates at different temperatures. This leads us to conclude that the system is intrinsically paramagnetic. Spin-glass-like behavior was proposed for $CaRuO_3$,[38] but we found no trace of static magnetic order in the sample by μSR as shown in Fig. 3(h). This result is consistent with a recent report of ^{99}Ru Mössbauer effect,[36] which also found no static magnetism.

The local field width Δ detected by μSR at $T = 2$ K changes apparently discontinuously in the calcium concentration interval $0.7 < x < 0.75$. The present study also demonstrated suppression of critical slowing down of dynamic spin fluctuations and phase separation around $x = 0.7$. These are typical behaviors expected for a first-order phase transition, and were also observed in MnSi[22] in applied pressure between the irreversibility on-set pressure p^* and the critical pressure p_c. The present results suggest that this may be a generic phenomenon near the quantum crossover from itinerant ferromagnet to correlated paramagnet. MnSi involves helical ordering due to lack of inversion symmetry of the B-20 crystals and Dzyaloshinskii-Moriya interaction. In contrast, the present system (Sr,Ca)RuO_3 does not involve these factors. Commonality of the results in these two systems promotes a notion that the observed first-order behavior is a generic property of itinerant ferromagnets.

In contrast to the abrupt change of the field width observed by μSR, a continuous change was observed in bulk magnetization as seen in Fig. 6, as the Ca concentration x is tuned through the magnetic transition. Magnetization is a volume-integrated parameter, which is proportional to the product of the local ordered moment size and the ordered volume fraction, while the μSR measurements can separately determine these two parameters. For elucidating evolution of local order parameter in spatially inhomogeneous systems, μSR has a definite advantage over volume-integrated methods, such as magnetization and neutron scattering.

As discussed in Ref. 22, first-order behavior was found not only in MnSi and (Sr,Ca)RuO_3, but in many systems including heavy fermions, high-T_c cuprates, superfluid He, and other systems. In general, one may expect first-order transitions when the free energy minimum occurs at finite value of the order parameter just above the transition temperature, which can be referred to as a "soft mode." This can be due to various different factors, such as, existence of competing order, effects of surface/boundary, and nucleation energies, etc. The SCR theory has so far been applied to second-order transitions, and no specific calculations have been performed for free energies of first-order transitions based on the SCR theory. Belitz *et al.*[54,55] reported that a first-order transition can be expected as generic phenomena due to the logarithmic term in the free energy in ferromagnets with itinerant electrons. The experimental results in MnSi and (Sr,Ca)RuO_3 are consistent with this theory, although they do not necessarily provide definitive proof.

In a recent study of Fe-doped MnSi, part of the present authors found a recovery of second-order behavior, presumably promoted by the randomness due to (Mn,Fe) substitutions.[56] This feature is also consistent with the theory of Belitz *et al.*, who discussed that randomness would suppress first-order behavior and promote recovery of second-order transitions. In this sense, it would be very interesting to revisit magnetic order of $CaRuO_3$ systems doped with various magnetic impurities (Ti, Fe, Mn, Ni, Cr, and Co) on the Ru site,[42–45] and elucidate their order of phase transitions.

The present work has also provided a clear evidence for the absence of static magnetic order in $CaRuO_3$. In $(Sr,Ca)_2RuO_4$, our recent μSR studies[57] have revealed that non-Fermi-liquid behavior in resistivity appears above the magnetic freezing temperature, suggesting that charge scattering via spin fluctuations as the origin of this behavior. Klein *et al.*[58] reported non-Fermi-liquid behavior in resistivity of $CaRuO_3$, with the $T^{1.5}$ dependence below $T \sim 50$ K. The absence of static magnetic order is consistent with this observation.

In summary, we have reported phase separation between magnetically ordered and paramagnetic volumes, associated with the suppression of dynamic critical behavior in $(Sr_{1-x}Ca_x)RuO_3$ near the phase boundary when the system evolves from ferromagnet to correlated paramagnet as a function of (Ca,Sr) substitution around the Ca concentration $x = 0.7$. Above $x = 0.7$, we found an extremely small static internal field suggestive of freezing of very dilute moments in a partial volume fraction at $x = 0.75$ and 0.8. We also confirmed that $CaRuO_3$ does not undergo static magnetic order above $T = 2$ K.

ACKNOWLEDGMENTS

This work has been supported by the US NSF under the Materials World Network (MWN: DMR-0502706 and 0806846), the Partnership for International Research and Education (PIRE: OISE-0968226), and DMR-1105961 programs

at Columbia, by Canadian NSERC and CIFAR at McMaster, and by the Japan-US Cooperative Science Program "Phase separation near quantum critical point in low-dimensional spin systems" Contract No. 14508500001 from JSPS of Japan at Kyoto. We wish to thank helpful discussions with Yoshiteru Maeno and Andrew Millis.

*Authors to whom correspondence should be addressed: imalureanu@sunymaritime.edu; tomo@lorentz.phys.columbia.edu

†Permanent address: National Research Council of Canada, Canadian Neutron Beam Centre, Chalk River Laboratories, Chalk River, Ontario K0J 1J0, Canada.

‡Permanent adress: National Institute of Advanced Industrial Science and Technology (AIST), 1-1-1 Central 2, Umezono, Tsukuba, Ibaraki, 305-8568, Japan.

§Permanent address: Oak Ridge National Laboratory, Oak Ridge, TN 37831, USA.

‖Permanent address: Dept. of Chemistry, University of Winnipeg Winnipeg, Maitoba, R3B 2E9, Canada.

[1] Y. Maeno, S. Nakatsuji, and S. Ikeda, Mater. Sci. Eng. B **63**, 70 (1999).

[2] B. V. Beznosikov and K. S. Aleksandrov, Cryst. Rep. **45**, 792 (2000).

[3] Y. Maeno, H. Hashimoto, K. Yoshida, S. Nishizaki, T. Fujita, J. G. Bednorz, and F. Lichtenberg, Nature (London) **372**, 532 (1994).

[4] A. P. Mackenzie and Y. Maeno, Rev. Mod. Phys. **75**, 657 (2003).

[5] J. J. Randall and R. Ward, J. Am. Chem. Soc. **81**, 2629 (1959).

[6] W. Bensch, H. W. Schmalle, and A. Reller, Solid State Ionics **43**, 171 (1990).

[7] H. Kobayashi, M. Nagata, R. Kanno, and Y. Kawamoto, Mater. Res. Bull. **29**, 1271 (1994).

[8] S. Nakatsuji and Y. Maeno, Phys. Rev. B **62**, 6458 (2000).

[9] S. Nakatsuji and Y. Maeno, Phys. Rev. Lett. **84**, 2666 (2000).

[10] R. J. Bouchard and J. L. Gillson, Mat. Res. Bull. **7**, 873 (1972).

[11] F. Fukunaga and N. Tsuda, J. Phys. Soc. Jpn. **63**, 3798 (1994).

[12] P. Rhodes and E. P. Wohlfarth, Proc. R. Soc. London A **273**, 247 (1963).

[13] T. Moriya, *Spin Fluctuations in Itinerant Electron Magnetism*, edited P. Fulde, Springer Series Solid State Science Vol. 56 (Springer-Verlag, Heidelberg, 1985).

[14] T. Moriya and A. Kawabata, J. Phys. Soc. Jpn. **34**, 639 (1973).

[15] T. Moriya and A. Kawabata, J. Phys. Soc. Jpn. **35**, 669 (1973).

[16] S. Doniach and S. Engelsberg, Phys. Rev. Lett. **17**, 750 (1966).

[17] K. K. Murata and S. Doniach, Phys. Rev. Lett. **29**, 285 (1972).

[18] G. G. Lonzarich and L. Taillefer, J. Phys. C: Solid State Phys. **18**, 4339 (1985).

[19] C. Pfleiderer, G. J. McMullan, S. R. Julian, and G. G. Lonzarich, Phys. Rev. B **55**, 8330 (1997).

[20] C. Pfleiderer, D. Reznik, L. Pintschovius, H. v. Löhneysen, M. Garst, and A. Rosch, Nature (London) **427**, 227 (2004).

[21] W. Yu, F. Zamborszky, J. D. Thompson, J. L. Sarrao, M. E. Torelli, Z. Fisk, and S. E. Brown, Phys. Rev. Lett. **92**, 086403 (2004).

[22] Y. J. Uemura, T. Goko, I. M. Gat-Malureanu, J. P. Carlo, P. L. Russo, A. T. Savici, A. Aczel, G. J. MacDougall, J. A. Rodriguez, G. M. Luke, S. R. Dunsiger, A. McCollam, J. Arai, Ch. Pfleiderer, P. Böni, K. Yoshimura, E. Baggio-Saitovitch, M. B. Fontes, J. Larrea J., Y. V. Sushko, and J. Sereni, Nat. Phys. **3**, 29 (2007).

[23] T. Kiyama, K. Yoshimura, K. Kosuge, Y. Ikeda, and Y. Bando, Phys. Rev. B **54**, 756(R) (1996).

[24] T. Kiyama, K. Yoshimura, K. Kosuge, H. Mitamura, and T. Goto, J. Phys. Soc. Jpn. **68**, 3372 (1999).

[25] A. Kanbayasi, J. Phys. Soc. Jpn. **44**, 108 (1978).

[26] T. Kiyama, K. Yoshimura, and K. Kosuge, in *Advances in Superconductivity IX*, Proceedings of the 9th International Symposium on Superconductivity (ISS'96), edited by S. Nakajima and M. Murakami (Springer, Berlin, 1996), Vol. 1, p. 171.

[27] T. Kiyama, K. Yoshimura, K. Kosuge, H. Michor, and G. Hilscher, J. Phys. Soc. Jpn. **67**, 307 (1998).

[28] M. Shikano, T. K. Huang, Y. Inaguma, M. Itoh, and T. Nakamura, Solid State Commun. **90**, 115 (1994).

[29] J. J. Neumeier, A. L. Cornelius, and J. S. Schilling, Physica B **198**, 324 (1994).

[30] J. J. Hamlin, S. Deemyad, J. S. Schilling, M. K. Jacobsen, R. S. Kumar, A. L. Cornelius, G. Cao, and J. J. Neumeier, Phys. Rev. B **76**, 014432 (2007).

[31] N. Kikugawa, L. Balicas, and A. P. Mackenzie, J. Phys. Soc. Jpn. **78**, 014701 (2009).

[32] K. Yoshimura, T. Imai, T. Kiyama, K. R. Thurber, A. W. Hunt, and K. Kosuge, Phys. Rev. Lett. **83**, 4397 (1999).

[33] H. Mukuda, K. Ishida, Y. Kitaoka, K. Asayama, R. Kanno, and M. Takano, Phys. Rev. B **60**, 12279 (1999).

[34] M. Daniel, J. I. Budnick, W. A. Hines, Y. D. Zhang, W. G. Clark, and A. R. Moodenbaugh, J. Phys. Condens. Matter **12**, 3857 (2000).

[35] N. Kolev, C. L. Chen, M. Gospodinov, R. P. Bontchev, V. N. Popov, A. P. Litvinchuk, M. V. Abrashev, V. G. Hadjiev, and M. N. Iliev, Phys. Rev. B **66**, 014101 (2002).

[36] M. Rams, R. Kmiec, M. Kruzel, Z. Swiatkowska, J. Gurgul, K. Krolas, and K. Tomala, J. Alloys Compd. **471**, 5 (2009).

[37] A. Koriyama, M. Ishizaki, T. C. Ozawa, T. Taniguchi, Y. Nagata, H. Samata, Y. Kobayashi, and Y. Noro, J. Alloys Compd. **372**, 58 (2004).

[38] I. Felner, I. Nowik, I. Bradaric, and M. Gospodinov, Phys. Rev. B **62**, 11332 (2000).

[39] R. Vidya, P. Ravindran, A. Kjekshus, H. Flellvag, and B. C. Hauback, J. Solid State Chem. **177**, 146 (2004).

[40] I. Felner and U. Asaf, Physica B **337**, 310 (2003).

[41] G. Cao, S. McCall, M. Shepard, J. E. Crow, and R. P. Guertin, Phys. Rev. B **56**, 321 (1997).

[42] T. He and R. J. Cava, Phys. Rev. B **63**, 172403 (2001).

[43] T. He and R. J. Cava, J. Phys. Condens. Matter **13**, 8347 (2001).

[44] A. Maignan, B. Raveau, V. Hardy, N. Barrier, and R. Retoux, Phys. Rev. B **74**, 024410 (2006).

[45] Y. Breard, V. Hardy, B. Raveau, A. Maignan, H.-J. Lin, L.-Y. Jang, H. H. Hsieh, and C. T. Chen, J. Phys. Condens. Matter **19**, 216212 (2007).

[46] The fit range of $1/\chi$ to the Curie Weiss law in $Sr_{1-x}Ca_xRuO_3$ is given in the following as [x; T_c; LT fit range; HT fit range]. [$x = 0$; $T_c = 154.5$ K; LT 161–200 K; HT 184–300 K], [0.30, 97 K; no LT fit; 140–300], [0.50; 37.6 K; 44–200; 150–300], [0.65; 14.8 K; 25–150; 150–300], [0.7; 13.0; 19–100; 100–300], and [0.8; no T_c; 2–85; 70–300].

[47]R. S. Hayano, Y. J. Uemura, J. Imazato, N. Nishida, T. Yamazaki, and R. Kubo, Phys. Rev. B **20**, 850 (1979).
[48]Y. J. Uemura, T. Yamazaki, D. R. Harshman, M. Senba, and E. J. Ansaldo, Phys. Rev. B **31**, 546 (1985).
[49]A. Keren, P. Mendels, I. A. Campbell, and J. Lord, Phys. Rev. Lett. **77**, 1386 (1996).
[50]S. J. Blundell, T. Lancaster, P. J. Baker, W. Hayes, F. L. Pratt, T. Atake, D. S. Rana, and S. K. Malik, Phys. Rev. B **77**, 094424 (2008).
[51]R. S. Hayano, Y. J. Uemura, J. Imazato, N. Nishida, T. Yamazaki, H. Yasuoka, and Y. Ishikawa, Phys. Rev. Lett. **41**, 1743 (1978).
[52]I. M. Gat-Malureanu, A. Fukaya, M. I. Larkin, A. J. Millis, P. L. Russo, A. T. Savici, Y. J. Uemura, P. P. Kyriakou, G. M. Luke, C. R. Wiebe, Y. V. Sushko, R. H. Heffner, D. E. MacLaughlin, D. Andreica, A. Shenck, and G. M. Kalvius, Phys. Rev. Lett. **90**, 157201 (2003).
[53]A. Ishigaki and T. Moriya, J. Phys. Soc. Jpn. **65**, 3402 (1996).
[54]D. Belitz, T. R. Kirkpatrick, and T. Vojta, Phys. Rev. Lett. **82**, 4707 (1999).
[55]D. Belitz, T. R. Kirkpatrick, and J. Rollbühler, Phys. Rev. Lett **94**, 247205 (2005).
[56]T. Goko *et al.* (unpublished).
[57]J. P. Carlo, T. Goko, I. M. Gat-Malureanu, P. L. Russo, A. T. Savici, A. A. Aczel, G. J. MacDougall, J. A. Rodriguez, T. J. Williams, G. M. Luke, C. R. Wiebe, Y. Yoshida, S. Nakatsuji, Y. Maeno, and Y. J. Uemura (unpublished).
[58]L. Klein, L. Antognazza, T. H. Geballe, M. R. Beasley, and A. Kapitulnik, Phys. Rev. B **60**, 1448 (1999).